Study of the solidification structure of compacted graphite cast iron

Marcos G. López, Graciela L. Rivera, Juan M. Massone & Roberto E. Boeri

Published online: 30 Sep 2016.

Submit your article to this journal

View related articles

View Crossmark data

Study of the solidification structure of compacted graphite cast iron

Marcos G. López ⓘD, **Graciela L. Rivera**, **Juan M. Massone** ⓘD* and **Roberto E. Boeri** ⓘD

This investigation focuses on the study of the solidification mechanism of compacted graphite cast iron (CGI). The solidification macrostructure was revealed in cast samples using a special technique known as direct austempering after solidification (DAAS). The microstructure was revealed by colour etching. The results were compared with earlier investigations of the solidification of spheroidal (SGI) and lamellar (LGI) graphite irons, and show that, similarly to other free graphite cast irons, the solidification of CGI is dominated by the presence of relatively large grains of austenite that can be observed with bare eyes. The CGI cast samples show a typical ingot structure, containing columnar and equiaxed grains, with a narrow columnar to equiaxed transition. The microstructure analysis showed that a dendritic substructure and a large number of eutectic colonies form the grains. Microsegregation is located inside the grains, mostly between secondary dendrite arms. The results indicate that the growth mechanism during solidification of CGI resembles that of LGI, but not the mechanism of SGI.

Keywords: Compacted graphite iron, solidification structure, DAAS technique, colour etching, solidification morphology

Introduction

Compacted graphite cast irons (CGI) are increasingly used, mainly in the automotive industry where the main current applications include diesel engine blocks, turbo housings, exhaust manifolds and brake components. CGI has excellent thermal fatigue resistance, and at present is replacing lamellar graphite iron in applications where greater mechanical strength is needed, as long as its lower thermal conductivity than flake graphite iron does not become a limiting factor. As the production of CGI is forecasted to increase over the next years, the basic understanding of its phase transformations becomes very important. Nowadays, the knowledge about the solidification behaviour of CGI is limited. Nevertheless, the prediction and prevention of casting defects such as micro-porosity demands a thorough understanding of the solidification of CGI.

Recent investigations about the solidification micro and macrostructures of spheroidal graphite cast iron (SGI) and lamellar graphite cast iron (LGI)[1–10] provided relevant information. Some key results were obtained after the application of specific colour etching techniques to examine the macro and microstructure of LGI and SGI.[2–5] This technique is sensitive to Si segregation and has proved to be effective to reveal the last to freeze areas (LTF) and primary dendrites in the microstructure of a cast iron sample.[2] It revealed the interaction between graphite and austenite in the eutectic colonies, allowing the authors to support the solidification model that was originally proposed by Rickert and Engler[1] for SGI.

In addition, another key technique was developed to reveal the solidification macrostructure of free graphite cast irons, named direct austempering after solidification (DAAS).[3,4]

DAAS allowed, for the first time, to reveal the ingot macrostructure of normally solidified SGI parts, showing the presence of grains of different size. Later, the correspondence of the observed grains with volumes of the same crystalline orientation was proved using electron backscattered diffraction on DAAS-treated samples of SGI and LGI.[11,12] DAAS was further employed by Elmquist et al.[6] to study the relation between shrinkage porosity and the solidification structure of LGI.

The results described above gave experimental support to an explanation of the solidification of these types of free graphite cast irons.[1,5,7] The proposal states that for both SGI and LGI, the solidification starts with the independent nucleation and growth of austenite dendrites and graphite from the melt. As dendrites grow, they interact with graphite particles, conforming solidification units that can be described as grains of austenite with a dendritic substructure that contain a very large number of graphite particles inside. This mechanism has also been proposed to be valid for hypo and hypereutectic free graphite irons.[3,4] Fig. 1 shows the solidification model proposed. Figure 1a shows a schematic of the eutectic solidification of LGI. It is observed that, after nucleating independently in the melt, flake graphite and austenite form units that grow cooperatively, with both phases in contact with the melt. These units are sometimes called 'eutectic colonies, cells or grains'. On the other hand, Fig. 1b represents a schematic of the solidification of eutectic SGI. An austenite layer envelops in this case spheroidal graphite particles soon after they get in contact with the growing austenite dendrites, and further growth of graphite is controlled by the diffusion of carbon from the melt to the graphite through the austenite shell. In both cases, it is found that as dendrites grow they contact each other, defining the austenite grain size. Each austenite grain contains a large number of graphite particles.

(a)

(b)
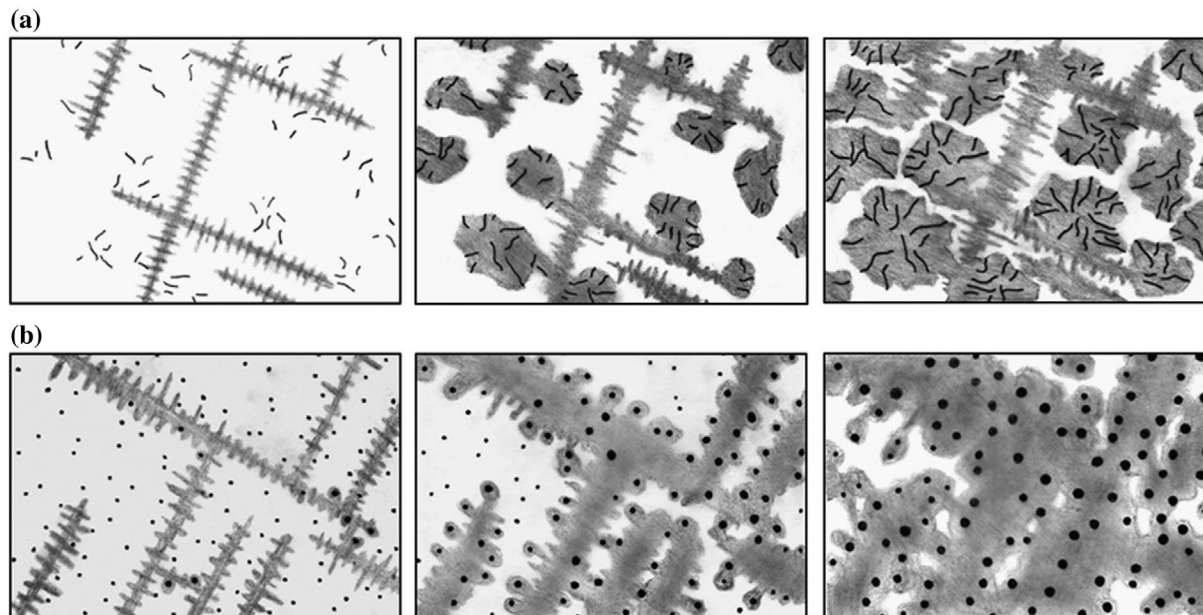
1 Schematic of the eutectic solidification of: *a* flake graphite cast iron; *b* spheroidal graphite cast iron.[11]
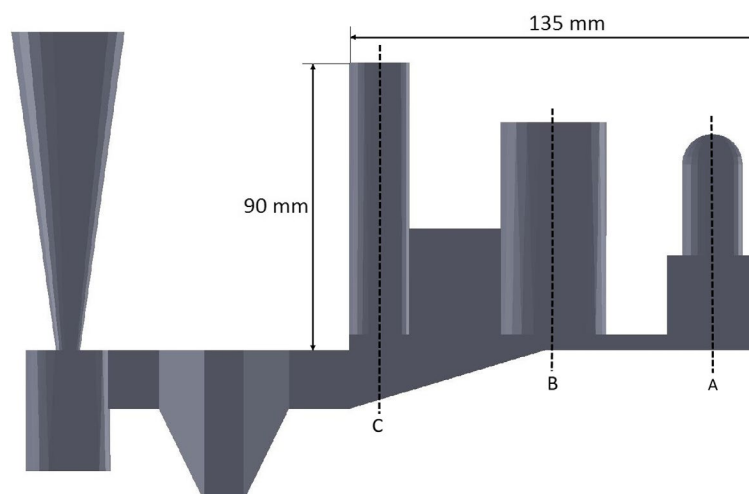
2 2D view of the pattern

For the case of CGI, studies of its solidification macro-structure and microsegregation are scarce. Loper et al.[13,14] conducted studies of the solidification of CGI by analysing samples quenched during solidification, determining that graphite precipitates in a spherical shape which degenerates during eutectic solidification and subsequently develops into compacted graphite. Mampaey[15] employed similar quenching experiments, finding that some of the compacted graphite particle tips remain in direct contact with the melt during eutectic solidification. This behaviour suggests that austenite and compacted graphite growth is coupled, in analogous manner of LGI. Recently Vazehrad et al.[16] have employed a colour etching technique as a tool to analyse and measure the eutectic colonies of coupled growth present in CGI samples with shrinkage porosity.

The revision of the literature specific for CGI suggests that the knowledge about the solidification mechanism of CGI could be improved by the application of new experimental techniques. Therefore, this investigation aims at characterising the macro and microstructures of compacted graphite iron by means of DAAS and colour etching, in order to advance in the understanding of CGI solidification.

Experimental procedure

All tests were carried out on samples obtained from cast iron heats made at the foundry laboratory of INTEMA. The castings included samples obtained using a pattern previously designed to study shrinkage cavities in cast iron,[17] as shown in Fig. 2.

Two experimental melts were prepared using a medium frequency induction furnace of 50 kg capacity. The chemical compositions of the heats are listed in Table 1. Melt A, with a CE of 4.29%, has eutectic composition, while Melt B is hypereutectic (CE = 4.58%). A standard melting procedure was used for all heats. After meltdown, the chemical composition was adjusted and the temperature was raised to 1500 °C, where the liquid metal was held for 10 min. Then, the melt

Table 1   Chemical compositions

Melt	%C	%Si	%Mn	%S	%P	%Mg	%Cu	%Ni
A	3.38	2.74	0.17	0.017	0.033	0.020	0.97	0.66
B	3.53	3.15	0.18	0.016	0.041	0.015	1.02	0.78
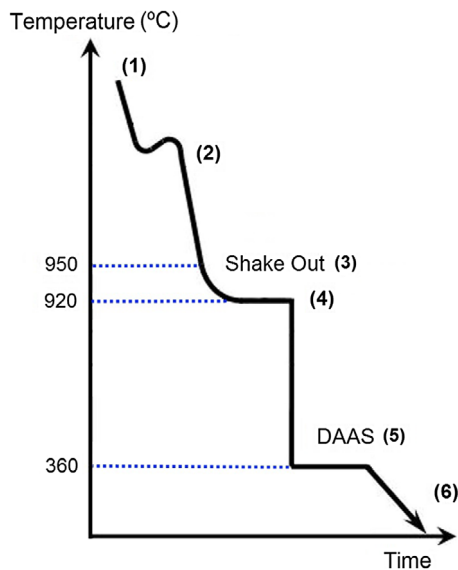
3   Plot of the stages in DAAS technique

was tapped into a 30-kg treatment ladle, where 0.6 wt% of FeSi6 Mg alloy was added through a sandwich-type treatment, while post inoculation was performed with 0.5 wt% of Fe–Si75%. Pouring temperature was 1400 °C. Compositions included small amounts of Cu and Ni that were added to reach the level of austemperability needed to perform the DAAS procedure.

The DAAS technique was applied to reveal the macrostructure of the CGI samples. The thermal cycle used is described in Fig. 3.

After pouring and solidification (Points 1 and 2 in Fig. 3), the cast parts were shaken out when their minimum temperature reached approximately 950 °C (Point 3), being then transferred to a furnace held at 920 °C, where they were kept during 30 min in order to allow their temperature homogenisation (Point 4). The parts were then austempered in a molten salt bath at 360 °C for 90 min (Point 5). Finally, they were cooled down to room temperature (Point 6). Later the samples were sectioned according to planes A, B and C in Fig. 2, polished and etched with Nital 2% to reveal the macrostructure.

As a last step, the solidification microstructure of the samples was revealed by colour etching using a solution composed by 10 g NaOH, 40 g KOH, 10 g picric acid and 50 ml of distilled water. Etching was carried out at the boiling temperature of the solution.

The nodularity rating was characterised by comparison with standard charts on the un-etched samples.

Results and discussion

Figure 4 shows the graphite morphology obtained in both melts. Graphite particles are mainly vermicular. The average of five fields per sample showed that Melt A has a nodularity of 30%, whereas Melt B has a nodularity of 15%. These values are consistent with the amounts of Mg found in each melt.

The microstructure of the metallic matrix after Nital 2% etching is shown in Fig. 5. The austempering heat treatment involved in the DAAS technique lead to a matrix microstructure formed by a fine mixture of acicular ferrite and austenite, which is usually called ausferrite.

The relatively high austempering temperature employed in the experimental procedure allowed to maximise the amount of retained austenite observed. This austenite is known as 'reacted austenite', and is part of the primary austenite that has been preserved in the matrix after the use of the DAAS technique.

The reacted austenite keeps the crystalline orientation defined during solidification. Therefore, after standard chemical etching, the grained structure of the austenite can be observed macrographically. Figures 6 and 7 show the macrostructures obtained after applying DAAS technique and etching with Nital 2% for Melts A and B, respectively. These are some of the first pictures published to date in which the solidification macrostructure of CGI is simultaneously shown with shrinkage porosity. Small equiaxed grains are visible at the faster solidifying portions of the sample, while much larger, and sometimes columnar grains are observed in other areas of the samples. In some cases, a sharp transition between columnar and equiaxial grains is observed.

When comparing the CGI macrostructures shown in Figs 6 and 7 with those obtained in earlier works by Rivera et al. for SGI and LGI,[5,8,11] their similarity becomes evident. Just as it was formerly concluded for spheroidal and flake
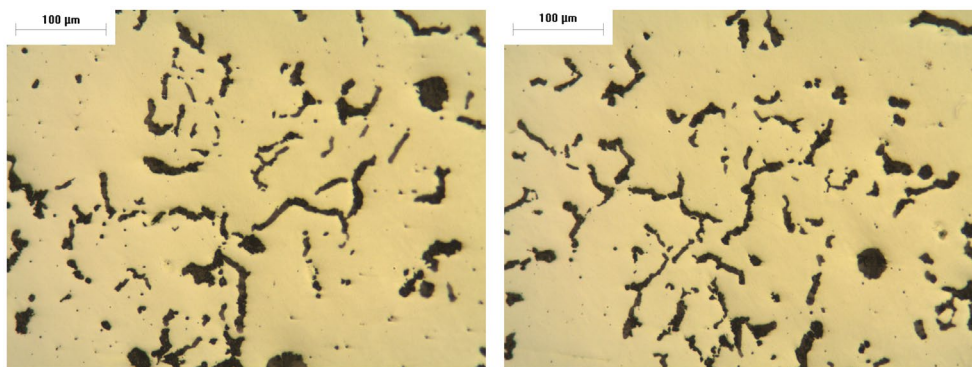
4   Microstructure of Melt A (left) and Melt B (right). Unetched
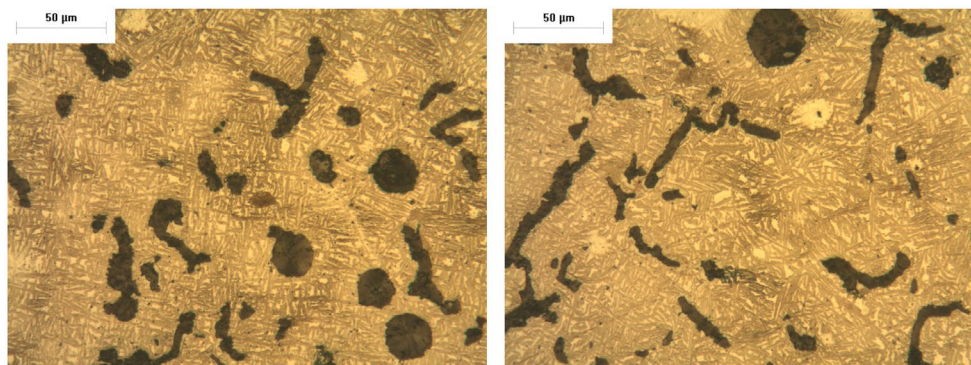
5   Microstructure of Melt A (left) and Melt B (right) after etching with Nital 2%

6   Solidification macrostructures of Melt A

7   Solidification macrostructures of Melt B

graphite irons, the appearance of very large austenite grains that contain a great number of graphite particles indicates that solidification of CGI is controlled by the nucleation and growth of austenite.

The results also show that the grain size is larger for the samples of the eutectic Melt A than that of the hypereutectic Melt B. This is clearly observed along the equiaxed grain

zone. This observation agrees with results previously obtained by Rivera et al. for SGI casting parts where it was found that hypereutectic samples show a smaller grain size than samples of eutectic composition.[4] The reasons for this behaviour are not completely understood, but it is possible that primary graphite particles present in the hypereutectic melt act at some extent as nucleation centres for austenite dendrites.

The examination of the microstructure of the melts after etching with a colour reagent shows the dendritic substructure of the austenite, Fig. 8. It is relevant to realise that almost all the area shown on Fig. 8 is included within a single grain of the columnar zones shown in Figs 6 and 7.

A closer look at the colour-etched microstructures of the melts allows locating the LTF zones through the identification of the silicon segregation. This is observed in Fig. 9, where the Si-depleted zones are the yellow, shiny areas frequently surrounding the dendrite arms. On the other hand, some relatively larger green areas have higher Si amounts, as pointed in Fig. 9. These green areas, some of them marked with white crosses in Fig. 10, correspond to the eutectic colonies that start growing from the primary austenite, involving coupled growth of austenite and vermicular graphite. As the size of these eutectic colonies is compared to the size of austenite grains found in macrostructures from Figs 6 and 7 it is found that many eutectic colonies are located inside a single austenite grain. This resembles the description of LGI solidification shown in Fig. 1.

A more detailed analysis of the sequence of colours in Fig. 10 shows that it represents the sequence of solidification, where the first to freeze areas are those in green, and the last to freeze those in yellow. Accordingly, Fig. 10 can be considered to be providing a snapshot of the sample while solidifying, being the solidification front represented by the interface between green and yellow zones (red areas). Under this assumption, it is seen that compacted graphite always grows towards the solidification front, keeping many times in direct touch with it. This fact has been pointed out in Fig. 11, where some vermicular graphite tips are visibly in touch with LTF zones (marked by white rectangles in Fig. 11). On the other hand, the graphite nodules present are always enveloped by a green shell (marked by black rectangles in Fig. 11), indicating that they were enveloped by a layer of austenite early during solidification since the austenite has high Si content.

These observations give support to explain the solidification of CGI in a similar manner of what has been proposed for LGI. After the initial nucleation and growth of austenite dendrites, cooperative growth between vermicular

8 Microstructure of Melt B showing the dendritic structure of the austenite. Colour etched
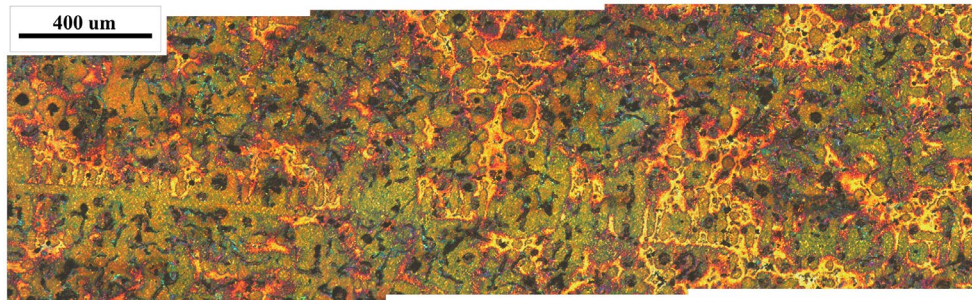
9 Microstructure of Melt B showing at higher magnification the LTF zones. Colour etched
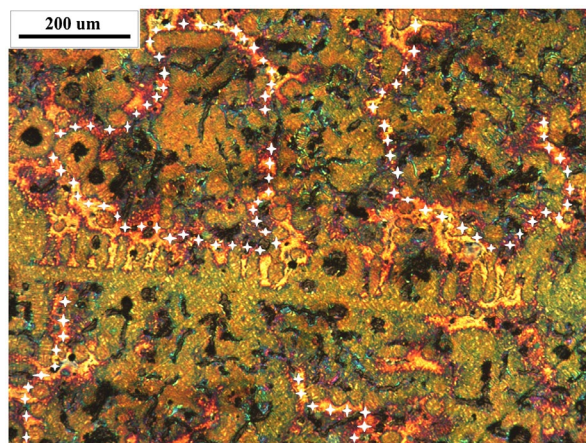
10 Zoom of microstructure where some eutectic colonies have been surrounded by white crosses

11 Zoom of microstructure. Black marked areas present graphite nodules enveloped by primary austenite. White marked areas show vermicular graphite particles in contact with LTF zones

graphite and austenite takes place, with both phases growing together in direct contact with the melt, composing the eutectic cells or colonies, as it was formerly proposed by Mampaey [15] in his analysis of partially solidified samples. This appears to be the case, regardless carbon equivalent value; since in a hypereutectic melt, such as Melt B, relatively large primary austenite dendrites from which the eutectic colonies or cells can grow are also found. This is different for the mechanism proposed for spheroidal graphite in which nodules are quickly surrounded by an austenite shell after they nucleate in the liquid, and have no further contact with the melt. [11]

Based on the observation of the micro and macrostructures shown in this study and the results of previous investigations, [9,11,15] it is proposed that the solidification of CGI proceeds in a similar way of LGI. The nucleation and growth of the austenite dendrites and graphite proceed independently in the melt. The graphite particles grow initially in the melt but later, as the growing austenite dendrites get in contact with them, form eutectic colonies in which austenite and graphite grow cooperatively, with both phases in contact with the melt. The portions of the casting exposed to higher cooling rates reach larger undercoolings and show a relatively large density of austenite nuclei, resulting in small grain size. On the other hand, slower cooling portions show smaller density of austenite nuclei and therefore larger grain size. Each one of these grains contains many eutectic colonies in it. A transition between columnar and equiaxial grains is observed in both heats for the different geometries poured.

The main features of the solidification of CGI revealed by this research are quite important for practical aspects. At the present time, the computational packages designed for the calculation of the filling and solidification of free graphite cast irons casting parts do not take into account the actual size and shape of the austenite dendrites, to the best of our knowledge. The prediction of fluid flow, filling, temperature evolution and defect formation should be improved by the implementation of more realistic solidification models.

Conclusions

1. The solidification of compacted graphite iron is dominated by the presence of relatively large grains of austenite that, after the use of the DAAS technique, can be observed by the naked eye, just as it was previously demonstrated for lamellar and spheroidal graphite cast irons. A clear columnar to equiaxial transition can be observed independently of carbon equivalent or casting geometry.
2. It is proposed that the solidification of CGI proceeds in a similar manner to that of LGI, namely with an initially independent nucleation and growth of austenite and graphite from the melt. Then, as solidification proceeds, a cooperative growth is established, forming eutectic colonies in which austenite and vermicular graphite grow together in direct contact with the melt.

Conflict of interest

No potential conflict of interest was reported by the authors.

Funding

ORCiD

López Marcos G. http://orcid.org/0000-0002-0494-7483
Massone Juan M. http://orcid.org/0000-0003-1287-1463
Boeri Roberto E. http://orcid.org/0000-0001-7083-579X

References

1. Rickert A, Engler S. "Solidification morphology of cast irons", the physical metallurgy of cast iron. *Mater. Res. Soc. Proc*. 1985;34:165–174.
2. Rivera G, Boeri R, Sikora J. Revealing the solidification structure of nodular iron. *Cast Met*. 1995;8:1–5.
3. Rivera G, Boeri R, Sikora J. Revealing and characterising solidification structure of ductile cast iron. *Mater. Sci. Technol*. June 2002;18:691–697.
4. Rivera G, Boeri R, Sikora J. Research advances in ductile iron solidification. *AFS Trans*. 2003;111:1–11.
5. Rivera G, Boeri R, Sikora J. Searching for a unified explanation of the solidification of cast irons. *Eighth Int. Symp. Sci. Process. Cast Iron Beijing China*. 2006;1:45–50.
6. Elmquist L, Diószegi A. Shrinkage porosity and its relation to solidification structure of grey cast iron parts. *Int. J. Cast Met. Res*. 2010;23:44–50.
7. Elmquist L, Diószegi A, Svidró P. Influence of primary austenite on the nucleation of eutectic cells. *Key Eng. Mater*. 2011;457:61–66.
8. Rivera G, Boeri R, Sikora J. Growth of eutectic austenite in free graphite cast irons. *Key Eng. Mater*. 2011;457:67–72.
9. Elmquist L, Soivio K, Diószegi A. Cast iron solidification structure and how it is related to defect formation. *Mater. Sci. Forum*. 2014;790–791:441–446.
10. Diószegi A, Fourlakidis V, Lora R. Austenite dendrite morphology in lamellar graphite iron. *Int. J. Cast Met. Res*. 2015;28:310–317.
11. Rivera G, Calvillo PR, Boeri R, Houbaert Y, Sikora J. Examination of the solidification macrostructure of spheroidal and flake graphite cast irons using DAAS and ESBD. *Mater. Charact*. 2008;59:1342–1348.
12. Elmquist L, Diószegi A, Björklind T. On the formation of shrinkage porosity in gray iron castings. *Key Eng. Mater*. 2011;457:416–421.
13. Pan E, Ogi K, Loper C. Analysis of the solidification process of compacted/vermicular graphite cast iron. *AFS Trans.*. 1982;90:509–527.
14. Li Y, Liu B, Loper C. Study of the solid–liquid interface during unidirectional solidification of cast iron. *AFS Trans*. 1990;98:483–488.
15. Mampaey F. Influence of compacted graphite on solidification morphology of cast iron. *AFS Trans*. 2000;27:11–17.
16. Vazehrad S, Elfsberg J, Diószegi A. On factors influencing macro shrinkage porosity formation in compacted graphite iron. *Mater. Sci. Forum*. 2014;790–791:429–434.
17. Tenaglia N, Boeri R, Rivera G, Massone J. Study of shrinkage porosity in spheroidal graphite cast iron. *Int. J. Cast Met. Res*. 2016;29:112–120.